2026 IEEE International Conference on Robotics and Automation (ICRA 2026)
June 1-5, 2026. Vienna, Austria

Field-Superimposed Control: Magnetically Driving Nanorobot Swarms with Hybrid Rotating and Gradient Fields

Chan Li[1,‡], Zijin Zeng[1,‡], Wenyan Niu[1], Jingwen Ye[1], Shunxiao Huang[1], Zaiyang Chen[1], Hongyan Sun[1], Yingjian Guo[1,†], Lin Feng[1,2,†]

***Abstract*— Magnetically actuated micro/nanorobot swarms have exhibited considerable promise for targeted biomedical delivery and localized therapies, attributed to their advantages of remote manipulation and robust penetration through biological tissues. However, achieving the simultaneous enhancement of both collective structural stability and efficient propulsion under a single-mode magnetic field remains a critical challenge. This paper presents a rotational–gradient superimposed magnetic actuation strategy that enables precise superposition of a uniform rotating field and a directional gradient magnetic field, using a tri-axial electromagnetic coil system. This approach significantly enhances the motility of micro/nanorobots while preserving their collective stability. Experimental results reveal that a co-directional gradient magnetic field can increase cluster velocity by 1.5-2 times without compromising cluster stability, while a counter-directional gradient magnetic field enables effective deceleration or anchoring of the swarm. Also, this paper elucidates the impact of the gradient magnetic field on swarm stability. Moreover, this paper demonstrates the formation of the chain-like structure of micro/nanorobots, which possess axial movement capability under the superimposed gradient magnetic field. This work provides a theoretical and experimental foundation for multi-field synergistic actuation of micro/nanorobot swarms, and paves new paths for their application in biomedical micromanipulation.**

I. INTRODUCTION

Magnetically actuated micro/nanorobots are emerging as a key technological approach for targeted transport and localized therapy in biological fluids[1], [2], [3], owing to their remote[4], penetrating[5], and biocompatible energy input mechanism[6]. Compared to individual microrobots, nanoscale superparamagnetic particles can self-assemble into nanorobot swarms (Narm) under external magnetic fields, exhibiting controllable morphologies and programmable collective behaviors. These swarms demonstrate enhanced robustness and scalability, especially in complex microenvironments such as near-wall regions[7], [8].

Nonetheless, achieving efficient and directional propulsion while maintaining stable and reproducible Narm structures remains a critical challenge. Uniform rotating magnetic fields can stably generate vortex-shaped clusters and facilitate morphological manipulation, but their translational propulsion efficiency is limited[9]. Applying gradient magnetic fields alone offers significant magnetophoretic driving force, yet often compromises the integrity of vortex structures and collective coherence[10]. Realizing cooperative rather than mutually interfering coupling control between these two field types represents a fundamental unresolved issue in the magnetic actuation of nanorobot swarms.

Extensive research has explored different magnetic field modalities[11]. For example, Dai et al. designed a gradient magnetic field generator based on a regular tetrahedral structure to control the locomotion of macrophage-based microrobots[12]. Xie et al. developed micro/nanorobots driven by rotating magnetic fields, demonstrating that adaptive changes in field direction can effectively alter the robots' morphology and layout to navigate narrow channels[13]. Jin et al. constructed a swarm of nanorobots actuated by oscillating magnetic fields, enabling reversible elongation of the swarm through control of its collective shape and motion states[14]. These studies collectively demonstrate the unique advantages of low-frequency, low-intensity magnetic fields in biomedical applications[15], [16], [17]. However, most existing strategies rely on a single field mode: gradient magnetic fields provide strong propulsion but lack fine-scale collective control, while rotating fields enhance structural stability but offer limited translational speed.

To address these challenges, this work proposes a superimposed rotating and gradient magnetic actuation strategy and a systematic analytical framework tailored for Narm. This paper developed a tri-axial electromagnetic coil system that enables independent regulation of currents in six coils, allowing for the tunable superposition of a uniform rotating magnetic field and an oriented gradient magnetic field in three-dimensional space. This combined field approach improves the swarm's propulsion speed without compromising its collective vortex structure.

First, this paper established a magnetic field model for the tri-axial coil system and conduct simulation analyses for both isolated and superimposed rotating and gradient magnetic fields. Second, this paper developed a theoretical force model describing Narm rolling along surfaces in static flow field, and use simulations to analyze the influence of swarm rolling on the surrounding fluid. Third, this paper investigated Narm

*This work was supported by the National Key R&D Program of China (Grant No. 2022YFF1502000), Beijing Municipal Fund for Distinguished Young Scholars (Grant No. JQ22022), and Fundamental Research Funds for the Central Universities (Grant No. YWF-22-K-101).

‡Chan Li and Zijin Zeng contributed equally to this work.

[1]School of Mechanical Engineering & Automation, Beihang University, Beijing 100191, China.

[2]Beijing Advanced Innovation Center for Biomedical Engineering, Beijing 102433, China.

†Corresponding authors: Yingjian Guo (e-mail: yingjguo@126.com) and Lin Feng (e-mail: linfeng@buaa.edu.cn).

locomotion under superimposed magnetic fields in static flow field. Experimental results reveal that under typical conditions (central magnetic flux density 6.3 mT, rotation frequency 50 Hz, gradient 2.2 mT/mm), a co-directional gradient can increase the propulsion speed by approximately 1.5–2 times without impairing vortex stability, while a counter-directional gradient enables reversible deceleration and anchoring. Notably, the anchoring field gradient required increases significantly with higher central magnetic flux density and rotation frequency. Fourth, this paper systematically examined the effect of gradient magnetic fields on Narm swarm stability. Experiments indicate that the gradient threshold for structural disruption rises with both central magnetic flux density and rotation frequency. Finally, this paper demonstrated the formation of chain-like Narm structures induced by a normal static magnetic field, as well as their rapid axial transport capability under the superimposed gradient.

Grounded in theoretical modeling, simulation, and experimental validation,this study demonstrates Narm manipulation under continuous hybrid magnetic fields, including controllable shape morphologies and distinct behavior control, constituting a new path for the collective actuation of nanorobot swarms.

II. SYSTEM AND CONTROL THEORY

A. System Configuration

In this study, a three-axis Helmholtz coil system is employed to generate multiple types of magnetic field modes, including rotating, gradient, and oscillating fields, as illustrated in Figure 1. The six electromagnetic coils are identical in specification, each with an outer diameter of 72 mm, an inner diameter of 40 mm, a length of 37 mm, and 170 turns.

A host computer control interface, developed using the C# programming language, enables users to set the type and intensity of the magnetic field. The system software calculates in real time the required input currents for the six coils, and stores the values in a buffer. The host computer communicates with an NI data acquisition card via a USB interface; the card reads current data from the buffer at hardware-timed intervals, converts the digital signals to analog outputs, and transmits them to the DC drivers. The drivers then amplify and stably deliver the current signals to the six coils, thereby generating the desired magnetic field configuration.A CCD camera provides real-time feedback on Narm motion state to the host computer, allowing experimenters to adjust the magnetic field parameters as needed and thereby achieve high-precision control over Narm locomotion.

To analyze the magnetic field distribution, COMSOL Multiphysics 6.3 was used to establish an electromagnetic coil model in this study. Given the complete symmetry of the system in the x, y, and z directions, the analysis of the three-dimensional magnetic field distribution was simplified to the xOy two-dimensional plane to highlight the key physical phenomena and results. The workspace was defined as a spherical region with a diameter equal to the inner diameter of the coil. By applying different currents, the magnetic field distribution in this plane was analyzed.

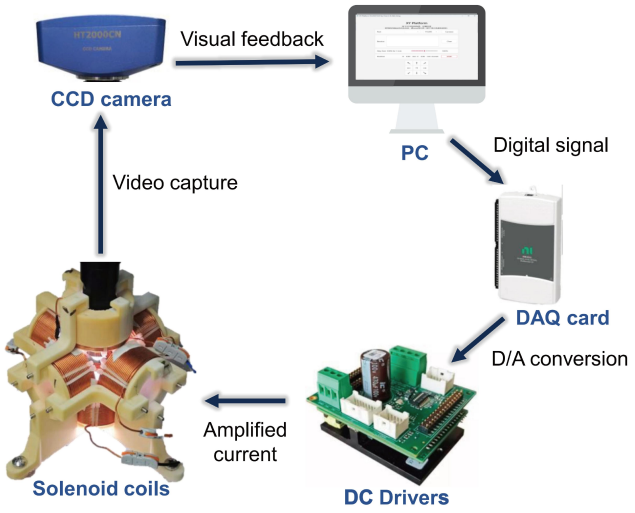

Fig. 1. Control System Diagram.

First, sinusoidal and cosinusoidal currents were supplied to the two sets of coils along the x and y axes, respectively, with equal current magnitude in each coil group. This configuration generates a rotating magnetic field in the xOy plane, which is used to drive Narm in a vortex-like motion. With the current amplitude set to 10 A, the simulation results are shown in Figure 2(a). It can be seen that the magnetic field is uniformly distributed within the workspace, with a central magnetic flux density of approximately 6 mT, and the magnetic field as rotates at the frequency of the supplied current.

When current is supplied only to the coil in the x+ direction, a gradient magnetic field is produced along that axis, as shown in Figure 2(b). The simulation results indicate that the magnetic field gradient increases in the positive x direction, reaching 1.5 mT/mm at the center of the workspace.

To produce a superimposed magnetic field, both rotating currents (sine and cosine) and gradient currents (single-direction sine or cosine component) were simultaneously applied to the coils in the x and y directions. This yields a superimposed rotational-gradient magnetic field in the xOy plane, as shown in Figures 2(c)-(f). The results show that the magnetic field in the workspace maintains a rotational profile, while also exhibiting a strong magnetic field gradient along the direction of rotation.

B. Force Analysis of Narm in Static Flow Field

In a static flow field environment, the net force resulting from gravity and buoyancy acting on the nanorobot is negligible compared to the magnetic force and viscous resistance. Therefore, within the parameter range of this study, the combined effect of gravity and buoyancy on in-plane motion can be ignored. The forces acting on the nanorobot are primarily categorized into three types:

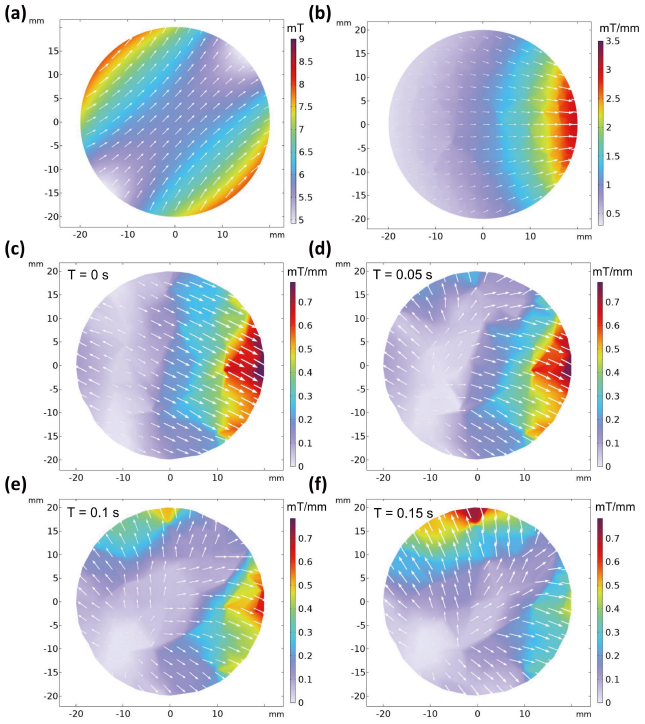

Fig. 2. Simulated magnetic field distributions of the control coils. (a) Rotating magnetic field; (b) Gradient magnetic field; (c)–(f) Superimposed rotating and gradient magnetic fields.

magnetic forces, hydrodynamic forces, and frictional forces. The overall force framework is illustrated in Figure 3.

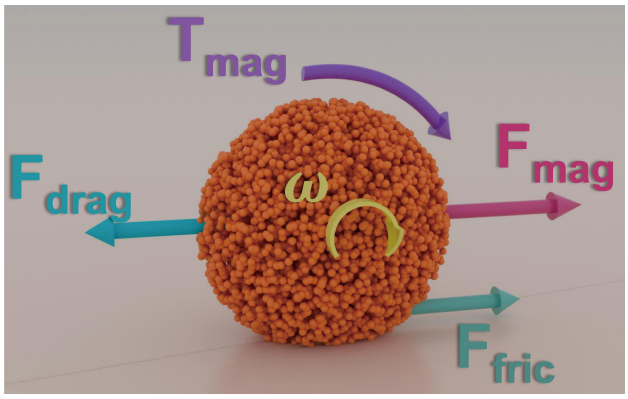

Fig. 3. Force Analysis of Narm in static flow field.

Among these, the magnetic forces mainly consist of the magnetic torque T_{mag} generated by the rotating magnetic field, and the magnetic force F_{mag} exerted by the gradient magnetic field:

$$\mathbf{T}_{\mathrm{mag}} = \mathbf{m} \times \mathbf{B}_{\mathrm{rot}} \tag{1}$$

$$\mathbf{F}_{\mathrm{mag}} = \nabla(\mathbf{m} \cdot \mathbf{B}_{\mathrm{grad}}) \tag{2}$$

Where $\mathbf{m}$ denotes the magnetic moment of the nanoparticle (A·m²), and $\mathbf{B}_{rot}$ represents the magnetic flux density vector of the rotating magnetic field (T). ∇ is the gradient operator, and $\mathbf{B}_{grad}$ denotes the magnetic flux density vector of the gradient magnetic field (T).

Under the influence of the magnetic torque, an individual nanorobot rotates in accordance with the external magnetic field, aligning its magnetic moment direction with that of the applied field. Upon activation of the rotating magnetic field, the nanorobots are rapidly magnetized and, due to the strong magnetic dipole–dipole interaction force F_{dipole}, connect end-to-end to form short chain-like structures:

$$\begin{aligned}\mathbf{F}_{\mathrm{dipole}} = \frac{3\mu_0}{4\pi r^4}[(\mathbf{m}_1 \cdot \mathbf{m}_2)\hat{\mathbf{r}} + (\mathbf{m}_1 \cdot \hat{\mathbf{r}})\mathbf{m}_2 \\ + (\mathbf{m}_2 \cdot \hat{\mathbf{r}})\mathbf{m}_1 - 5(\mathbf{m}_1 \cdot \hat{\mathbf{r}})(\mathbf{m}_2 \cdot \hat{\mathbf{r}})\hat{\mathbf{r}}]\end{aligned} \tag{3}$$

Here, μ_0 is the vacuum permeability ($4\pi \times 10^{-7}$ N/A²), r is the distance between two particles (m), $\mathbf{m}_1$ and $\mathbf{m}_2$ are the magnetic moments of the two particles (A·m²), and $\hat{r}$ is the unit vector along the line connecting the two particles.

The rotating magnetic field applies a magnetic torque to each short chain, driving it to continuously rotate like a microscopic magnetic stir bar. Meanwhile, under the effect of the magnetic dipole–dipole force, these short chains further assemble into longer chains, eventually resulting in an overall vortex-like motion of Narm.

Under the influence of the magnetic force, a single nanorobot tends to move along the direction of the steepest magnetic field gradient. In the presence of only a gradient magnetic field, such movement is difficult to control effectively at the microscale. However, once Narm has formed a stable vortex motion, superimposing a gradient magnetic field along the direction of motion enables the entire Narm to achieve higher propulsion speeds while maintaining collective vortex behavior.

When nanorobots move in static flow field, the fluid forces they experience mainly include Stokes drag, Brownian force, added mass force, and the Basset history force. Since Narm operates in a creeping flow regime with an extremely low Reynolds number, both the added mass force and Basset history force can be neglected. In the presence of a strong magnetic field, the magnetic force dominates, rendering the Brownian force negligible as well. Therefore, the primary fluid dynamic force acting on Narm is the Stokes drag force (F_{drag}), which acts in the direction opposite to the relative motion of Narm with respect to the fluid and serves to impede its movement:

$$\mathbf{F}_{\mathrm{drag}} = -6\pi\eta R(\mathbf{v}_{\mathrm{particle}} - \mathbf{v}_{\mathrm{fluid}}) \tag{4}$$

Here, η denotes the dynamic viscosity of the fluid (Pa·s), R is the hydrodynamic radius of the nanoparticle (m), $v_{particle}$ is the velocity of the particle (m/s), and v_{fluid} is the velocity of the fluid (m/s).

During Narm's motion, the frictional force manifests as a wall friction torque. This torque not only increases motion resistance but also provides additional thrust when Narm rolls along the wall.

To analyze the effect of Narm's motion on the surrounding fluid, COMSOL Multiphysics 6.3 was used for modeling and simulation. Since Narm maintains a stable structure during its vortex-like rotational motion, it can be approximated as a rigid body over this period.The simulation results are shown

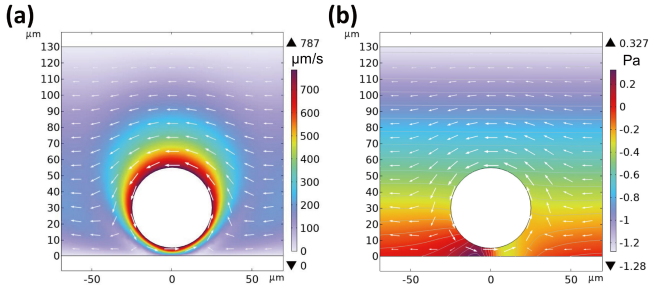

Fig. 4. Influence of Narm motion in static flow field on (a) fluid velocity and (b) pressure.

in Figure 4: when Narm rotates counterclockwise, it drives the surrounding fluid to flow in the negative x-direction, exerting a positive pressure on the fluid ahead of the rotation, and creating a negative pressure effect behind it.

III. EXPERIMENTS AND RESULTS

A. Regulation of Swarm Morphology by Gradient Magnetic Field

In this study, superparamagnetic Fe_3O_4 nanoparticles with a diameter of 300 nm were used as the experimental subjects. Polystyrene microspheres with a diameter of 3 μm were introduced as tracer particles to observe the motion of Narm under the combined action of a gradient magnetic field and rotating magnetic field, as well as the disturbances induced in the surrounding flow field. The concentration of Fe_3O_4 nanoparticles was set at 0.5 mg/mL, while the concentration of polystyrene microspheres was 25 mg/mL. The two components were uniformly mixed at a volumetric ratio of 100:1. For each experiment, 15 μL of the mixed solution was dropped onto a glass slide, then covered with a coverslip and maintained at a 300 μm gap to prevent evaporation. The sample was positioned at the center of the coil system's workspace for observation.

When only a rotating magnetic field was applied, Narm exhibited a vortex-like rolling motion due to the magnetic torque (Figure 5(a)). In contrast, when only a gradient magnetic field was applied, nanoparticles as a whole moved in the direction of increasing magnetic field gradient. However, due to the absence of a significant swarm structure and the low particle concentration, this movement was difficult to observe clearly under an optical microscope (Figure 5(b)). To highlight the effect of the gradient magnetic field, the rotating magnetic field was switched off immediately after Narm established a stable vortex motion, and a gradient magnetic field was subsequently applied. Under these conditions, the directed migration of Narm along the field gradient could be observed (Figure 5(c)).

By superimposing gradient magnetic fields of different magnitudes, directions, and types onto the rotating magnetic field, an asymmetric magnetic field distribution can be generated within the workspace. This modifies the position of the vortex center and enables control over the various motion modes exhibited by Narm. With increasing gradient

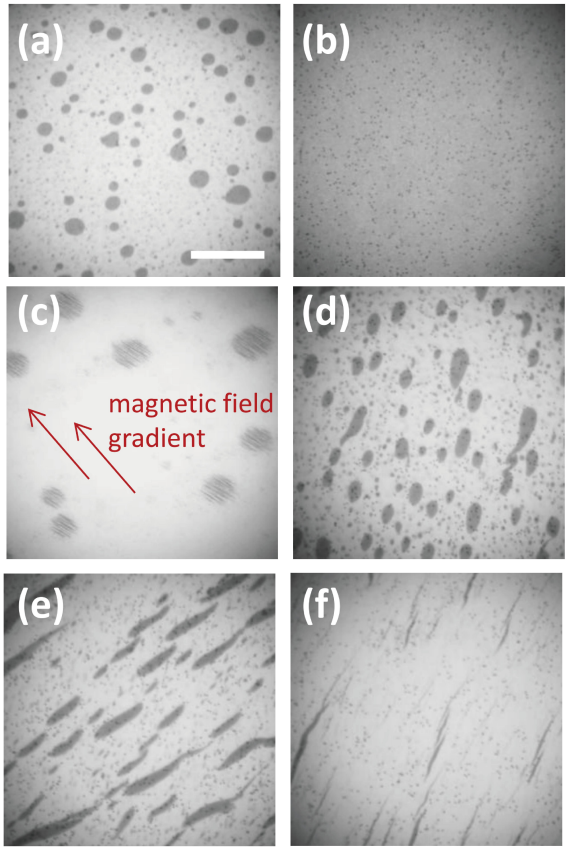

Fig. 5. Various motion modes of Narm. (a) Controlled by rotating magnetic field only: vortex-like motion. (b) Controlled by gradient magnetic field only: no swarm formation. (c) Application of gradient magnetic field immediately after switching off rotating magnetic field: directional motion of Narm along the field gradient is observed. (d)–(f) Under simultaneous control of rotating and gradient magnetic fields: Narm exhibits spindle-shaped, strip-shaped, and linear motions. Scale bar: 200 μm.

magnetic field strength, the morphology of Narm gradually evolves from a vortex shape to spindle-like, strip-like, and linear structures (Figure 5(d–f)).

When the gradient magnetic field is modulated to oscillate rapidly across the workspace, the structural stability of Narm is disrupted, leading to the dispersion of the swarm; the cluster can then be reconstructed under the continuous action of the rotating magnetic field (Figure 6(a)). Here, the disruption of the structural stability is identified by the onset of a wave-like morphology accompanied by swarm dispersion. In contrast, when the gradient magnetic field is modulated at a lower frequency, Narm is not completely disrupted, but instead splits into several smaller sub-clusters (Figure 6(b)).

The fusion and exchange processes between Narm modules can be clearly observed with the aid of tracer particles. When two Narm modules approach each other, particle exchange occurs due to the vortex-induced advective effect (long-range attractive interaction) (Figure 7(a)). As the distance further decreases, the particles enter a fusion region and form an irregular vortex. Eventually, through a diffusion-driven mechanism, the system reorganizes into a

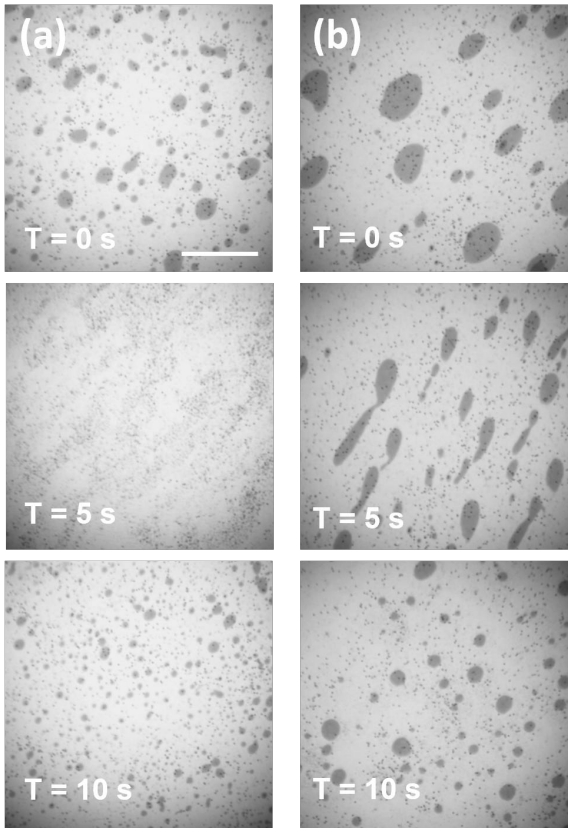

Fig. 6. Combination of rotating magnetic field and (a) high-frequency oscillating gradient magnetic field, enabling disruption and reformation of the Narm vortex structure; (b) low-frequency oscillating gradient magnetic field, leading to the splitting of the Narm vortex structure. Scale bar: 200 μm.

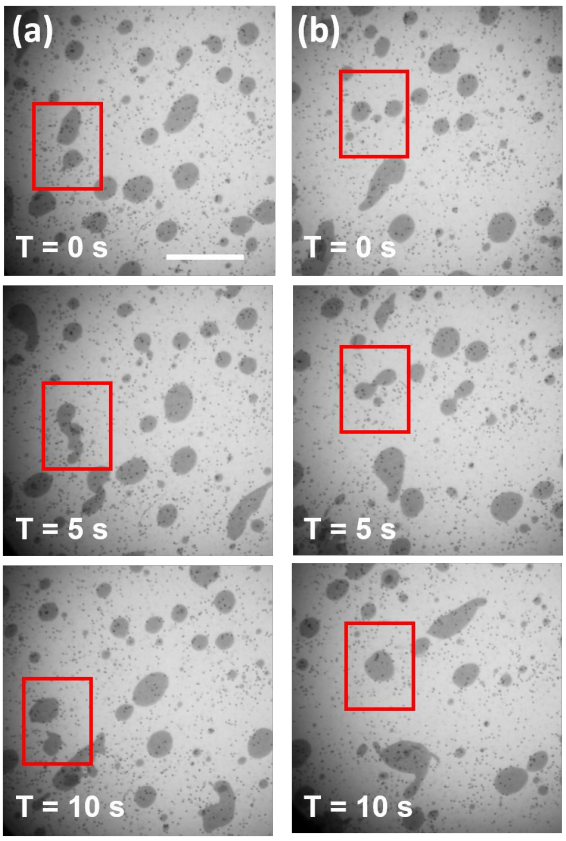

Fig. 7. (a) Exchange and (b) fusion processes of Narm. Scale bar: 200 μm.

regular vortex structure (Figure 7(b)).

B. Regulation of Motion Speed by Gradient Magnetic Fields

On the basis of maintaining Narm vortex motion using a rotating magnetic field, applying gradient magnetic fields of varying strengths and directions enables control over the speed and position of the Narm modules. When the direction of the gradient magnetic field is aligned with the direction of Narm movement, the collective motion accelerates (Figure 8(a)); conversely, when the direction is opposite, the movement slows down or the modules are anchored in place (Figure 8(b,c)). Here, an anchored swarm is defined as maintaining a maximum centroid displacement below one-tenth of its diameter within a 1 s time window.

This paper systematically investigated the influence of gradient magnetic fields on the motion speed of Narm. When the central magnetic flux density was maintained at 6.3 mT and the gradient strength at 2.2 mT/mm, the velocity of Narm increased with the frequency of the rotating magnetic field, and the presence of a co-directional gradient magnetic field enhanced the speed by up to 1.5 times (Figure 9(a)). Under a fixed rotation frequency of 50 Hz and a gradient strength of 2.2 mT/mm, the Narm velocity increased with the central magnetic flux density, and the gradient magnetic field resulted in a significant acceleration effect, boosting the speed by 1.5–2 times (Figure 9(b)). Notably, when the central magnetic flux density was below 3 mT, the effect of the gradient magnetic field far exceeded that of the rotating field, causing the cluster motion to become unsustainable. When the rotation frequency was fixed at 50 Hz and the central magnetic flux density at 6.3 mT, the Narm velocity initially increased slowly and then rose sharply with increasing gradient magnetic field strength (Figure 9(c)).

In addition, this study analyzed the relationship between the magnetic field gradient required to anchor Narm and the central magnetic flux density and frequency of the rotating magnetic field (Figure 10). The results show that as the central magnetic flux density and the rotation frequency increase, the magnetic field gradient required for anchoring initially increases slowly and then rises sharply. The underlying reason is that higher Narm motion velocity leads to greater kinetic energy and momentum; thus, a stronger gradient magnetic field is required to maintain cluster stability or to change its motion state, such as anchoring.

C. Influence of Gradient Magnetic Field on Vortex Stability

When the effect of the gradient magnetic field surpasses that of the rotating field, the stability of the Narm cluster is compromised (Figure 11(a)). To quantitatively assess Narm's

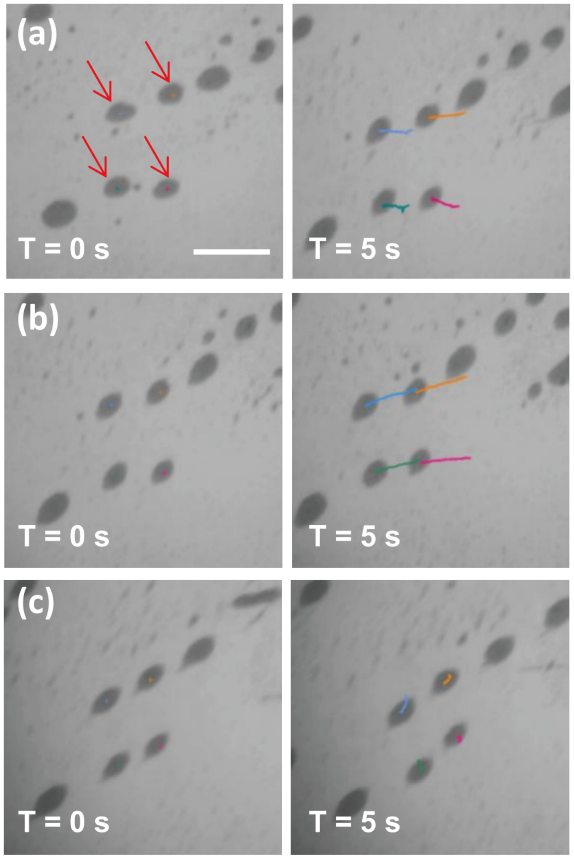

Fig. 8. Processes of (a) deceleration, (b) acceleration, and (c) anchoring of Narm under gradient magnetic fields. Scale bar: 100 μm.

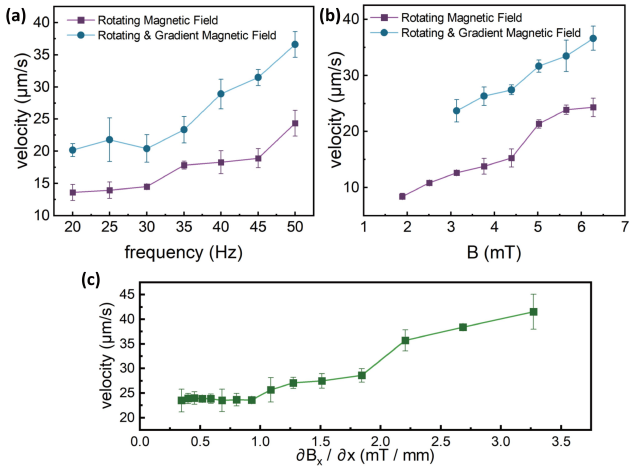

Fig. 9. Relationship between Narm motion velocity and (a) rotating magnetic field frequency, (b) central magnetic flux density, and (c) magnetic field gradient.

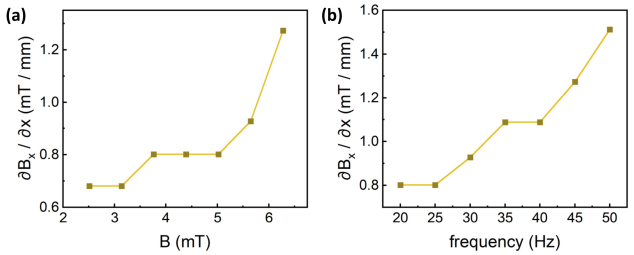

Fig. 10. Relationship between the gradient magnetic field required for anchoring Narm and (a) the central magnetic flux density and (b) the frequency of the rotating magnetic field.

structural stability, the magnetic field gradient required to disrupt the cluster was measured. The transition from a linear to a wave-like morphology was set as the criterion for instability, and the critical gradient magnetic field strength under various central magnetic flux densities and rotational frequencies was experimentally determined (Figure 11(b,c)). The results indicate that the magnetic field gradient required to destabilize the cluster increases with central magnetic flux density and rotational frequency, suggesting that the stability of the Narm cluster is enhanced under higher values of these parameters.

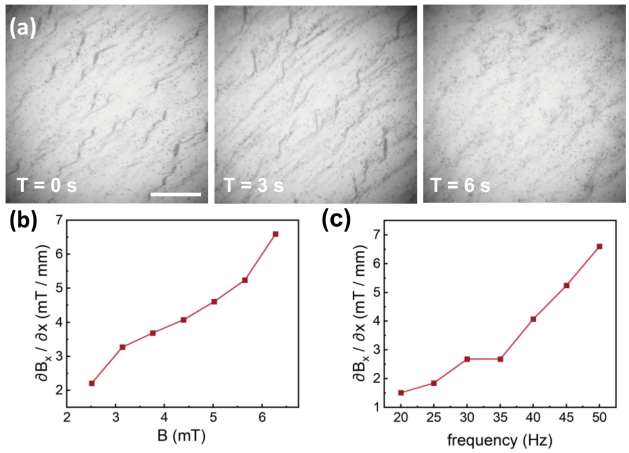

Fig. 11. The stability of Narm. (a) Narm cluster undergoes disruption, leading to a significant change in state. Scale bar: 200 μm. As the (b) central magnetic flux density and (c) rotational frequency increase, the magnetic field gradient required to disrupt the cluster also increases.

Experimental results demonstrate that Narm is not simply a loose assembly of particles, but rather a dynamic structure with intrinsic mechanical strength. As the central magnetic flux density increases, the magnetization intensifies and the dipole–dipole interactions between particles become significantly stronger, thus necessitating a higher gradient magnetic field to induce disruption. Similarly, higher rotating field frequencies cause the Narm vortex to rotate more rapidly, which generates an inward force on surrounding fluid that compresses and tightens the cluster, resulting in a denser and more stable structure that resists destruction.

D. Motion Control and Transport Applications of Chain-like Structures

A static magnetic field applied perpendicular to a rotating magnetic field can induce Narm to form chain-like structures (Figure 12(a)). On this basis, applying a moderate axial gradient magnetic field enables the chain-like structure to simultaneously undergo radial rolling and axial translation; when the chain length exceeds a certain threshold, the rolling effect becomes negligible and axial translation dominates. The motion pattern can be clearly confirmed by tracking the trajectories of tracer particles (Figure 12(b)). This finding offers a new approach for the directional transport of Narm in narrow channels, such as microvessel.

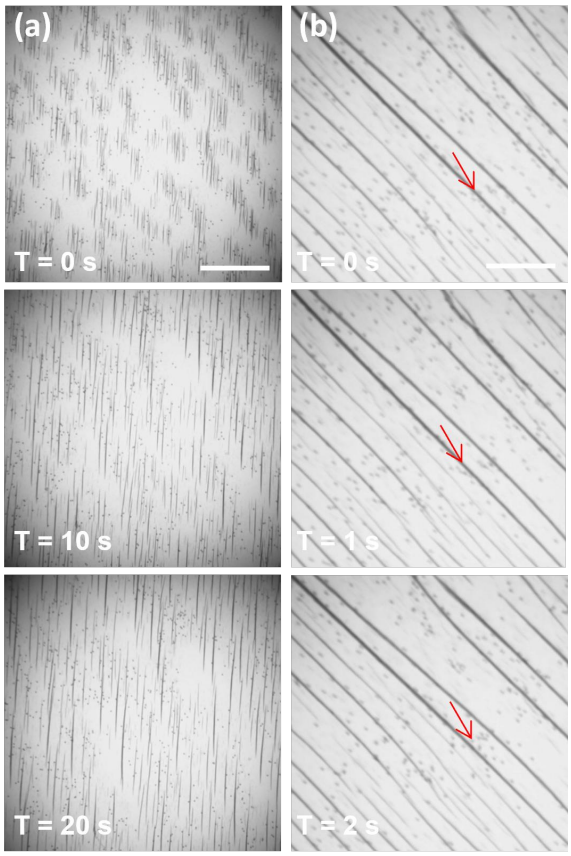

Fig. 12. Chain-like motion of the Narm cluster: (a) Formation process of the chain, scale bar: 100 μm; (b) Tracer particles confirm rolling and translation of the chain, scale bar: 200 μm.

IV. CONCLUSIONS

This study proposes a rotational–gradient superimposed magnetic actuation method for nanorobot clusters, effectively addressing the challenge of balancing stability and propulsion efficiency in traditional single-field-driven systems. By constructing a triaxial coil system and a multiphysics field coupling model, precise control over the motion modes and velocity of Narm was achieved. Experimental results demonstrate that imposing a co-directional gradient magnetic field significantly enhances cluster velocity, while a counter-directional gradient magnetic field enables controlled deceleration and anchoring. Furthermore, as cluster stability increases, the magnetic field gradient required to disrupt the cluster also rises. In addition, this study presents the formation of chain-like structures induced by static magnetic fields and their axial transport capabilities under gradient magnetic fields, offering new paths for directional motion in narrow environments such as microvessel. This work not only establishes a theoretical and experimental framework for multiphysics field-superimposed actuation of Narm, but also lays the foundation for high-precision control in future biomedical applications of micro/nanorobots, including targeted drug delivery and minimally invasive surgery.

REFERENCES

[1] B. J. Nelson and S. Pané, "Delivering drugs with microrobots," Science, vol. 382, no. 6675, pp. 1120–1122, Dec. 2023.

[2] Y. Seol et al., "Stimuli-triggered pollen-inspired micro/nanorobots for advanced therapeutics," Nano Today, vol. 57, p. 102337, Aug. 2024.

[3] M. Hu, X. Ge, X. Chen, W. Mao, X. Qian, and W.-E. Yuan, "Micro/Nanorobot: A Promising Targeted Drug Delivery System," Pharmaceutics, vol. 12, no. 7, p. 665, Jul. 2020.

[4] Z. Zeng, F. Wang, C. Li, M. Tan, S. Wang, and L. Feng, "Dung Beetle Optimizer-based High-precision Localization for Magnetic-Controlled Capsule Robot," in 2024 IEEE/RSJ International Conference on Intelligent Robots and Systems (IROS), Abu Dhabi, United Arab Emirates: IEEE, Oct. 2024, pp. 2347–2352.

[5] B. Wang, K. Kostarelos, B. J. Nelson, and L. Zhang, "Trends in Micro-/Nanorobotics: Materials Development, Actuation, Localization, and System Integration for Biomedical Applications," Advanced Materials, vol. 33, no. 4, p. 2002047, Jan. 2021.

[6] C. Li, Z. Hu, H. Sun, C. Wang, Z. Zeng, and L. Feng, "Magnetically Controlled Nanorobotic Swarm for the Glioma Therapy," in 2023 WRC Symposium on Advanced Robotics and Automation (WRC SARA), Beijing, China: IEEE, Aug. 2023, pp. 420–425.

[7] C. Li et al., "Multimodal Upstream Motion of Magnetically Controlled Micro/Nano Robots in High-Viscosity Fluids," in 2025 IEEE/RSJ International Conference on Intelligent Robots and Systems (IROS), Hangzhou, China: IEEE, Oct. 2025, pp. 801–806.

[8] L. Wang et al., "Reconfigurable Vortex-like Paramagnetic Nanoparticle Swarm with Upstream Motility and High Body-length Ratio Velocity," Research, vol. 6, p. 0088, Jan. 2023.

[9] L. Wang, C. Gan, H. Sun, and L. Feng, "Magnetic nanoparticle swarm with upstream motility and peritumor blood vessel crossing ability," Nanoscale, vol. 15, no. 34, pp. 14227–14237, 2023.

[10] B. Wang et al., "Spatiotemporally Actuated Hydrogel by Magnetic Swarm Nanorobotics," ACS Nano, vol. 16, no. 12, pp. 20985–21001, Dec. 2022.

[11] H. Zhou, C. C. Mayorga-Martinez, S. Pané, L. Zhang, and M. Pumera, "Magnetically Driven Micro and Nanorobots," Chem. Rev., vol. 121, no. 8, pp. 4999–5041, Apr. 2021.

[12] Y. Dai et al., "Precise Control of Customized Macrophage Cell Robot for Targeted Therapy of Solid Tumors with Minimal Invasion," Small, vol. 17, no. 41, p. 2103986, Oct. 2021.

[13] H. Xie et al., "Reconfigurable magnetic microrobot swarm: Multimode transformation, locomotion, and manipulation," Sci. Robot., vol. 4, no. 28, p. eaav8006, Mar. 2019.

[14] D. Jin, J. Yu, K. Yuan, and L. Zhang, "Mimicking the Structure and Function of Ant Bridges in a Reconfigurable Microswarm for Electronic Applications," ACS Nano, vol. 13, no. 5, pp. 5999–6007, May 2019.

[15] Z. Zeng, F. Wang, J. Zhao, C. Wang, C. Li, and L. Feng, "The Control System for 5-DOF Magnetic Levitation Capsule Robot," in 2023 WRC Symposium on Advanced Robotics and Automation (WRC SARA), Beijing, China: IEEE, Aug. 2023, pp. 174–179.

[16] L. Wang et al., "Micro-Nanocarriers Based Drug Delivery Technology for Blood-Brain Barrier Crossing and Brain Tumor Targeting Therapy," Small, vol. 18, no. 45, p. 2203678, Nov. 2022.

[17] D. Ahmed, T. Baasch, N. Blondel, N. Läubli, J. Dual, and B. J. Nelson, "Neutrophil-inspired propulsion in a combined acoustic and magnetic field," Nat Commun, vol. 8, no. 1, p. 770, Oct. 2017.